Environ Monit Assess (2023) 195:221
https://doi.org/10.1007/s10661-022-10493-y

Development and validation of an open-source four-pole electrical conductivity, temperature, depth sensor for in situ water quality monitoring in an estuary

J. Wesley Lauer · Piper Klinger · Scott O'Shea · Se-Yeun Lee

Received: 17 December 2021 / Accepted: 10 September 2022 / Published online: 21 December 2022

Abstract Most recent implementations of low-cost electrical conductivity (EC) sensors intended for water quality measurements are based on simple two-pole designs. However, in marine settings, EC often exceeds the range where two-pole sensors provide reliable results. We have developed a simple four-pole EC sensor that relies exclusively on analog-to-digital measurements made using readily available circuit boards (pyboard v.1.1 or Raspberry Pi Pico 2040) programmed using MicroPython. Other than resistors and graphite or wire electrodes, no other electronic components are required for the EC sensor. When combined with a pressure/temperature sensor (MS5803-05), an optional NTC thermistor, batteries, and a waterproof housing constructed using a PVC pipe and a 3-D-printed cap, the device becomes a working conductivity-temperature-depth sensor capable of extended field deployments. Construction is sufficiently simple that undergraduate science students can construct one during three 3-h lab periods. Lab calibrations performed on several prototypes at ECs between 0.18 and 45 mS/cm show that confidence limits as good as about ±3% of EC are possible. Re-calibration of several prototypes 1 year after initial calibration shows that long-term calibration drift is modest. Data collected by the prototypes over several tidal cycles in the Duwamish River, Washington, USA, are in agreement with data from a co-located commercial YSI-EX03 conductivity probe. When distributed across a constructed off-channel wetland in the Duwamish system, the sensors documented large amounts of spatial and temporal variability in EC, highlighting the importance of such wetlands for providing unique temperature/salinity environments potentially valuable for outmigrating juvenile salmon.

Keywords Low-cost sensor · Electrical conductivity · CTD · MicroPython · Estuarine circulation

J. W. Lauer (✉)
Department of Civil & Environmental Engineering, Seattle University, 901 12th Avenue, Seattle, WA 98122, USA
e-mail: lauerj@seattleu.edu

P. Klinger · S.-Y. Lee
Department of Civil & Environmental Engineering, Seattle University, Seattle, WA 98122, USA

Present Address:
P. Klinger
U.S. Army Corps of Engineers, Seattle, WA 98134, USA

Present Address:
P. Klinger
Department of Civil & Environmental Engineering, University of Washington, Seattle, WA 98195, USA

S. O'Shea
Department of Electrical Engineering, Seattle University, Seattle, WA 98122, USA

Present Address:
S. O'Shea
Association for Energy Affordability, Emeryville, CA 94608, USA

Introduction

The use of electrical conductivity (EC) measurements for characterizing salinity and water quality is of fundamental importance in oceanography, hydrology, and water resources management. In some situations, EC varies only modestly around a base value that may be quite high (in the case of seawater) or quite low (in the case of direct precipitation). On the other hand, in estuaries and tidal rivers, tide-driven exchange of marine and river water can cause EC to vary across orders of magnitude on hourly timescales. While commercial EC sensors have long been available for use in these environments, cost can be a barrier, particularly among educators or citizen science groups who may not have the resources to acquire research-grade instrumentation.

Recent developments in open-source electronics have made low-cost environmental sensors accessible to an increasingly wide audience (Mao et al., 2019; Beddows et al., 2018; Blackstock et al., 2019; DeBell et al., 2019; Seroy et al., 2020; Chan et al., 2020; Mendez-Barroso et al., 2020; Levine et al., 2020). Platforms such as Arduino and MicroPython allow microcontrollers to collect data from an enormous range of commercially available environmental sensors, often with only modest programming effort. Libraries for logging data from low-cost sensors are available on curated websites such as EnviroDIY.org and from a number of commercial suppliers (e.g., Adafruit's libraries at CircuitPython.org or SparkFun's Artemis libraries). Microcontrollers themselves usually include the ability to sense voltage using built-in analog-to-digital converters (ADCs), and in some cases, built-in timers and other on-board sensors support measurement of environmental parameters without any additional electronics. 3-D printing and/or laser-cutting technology allows for precise manufacturing of non-electronic components of sensing systems. Well-designed systems can run autonomously for months, regularly logging sensor readings to on-board flash memory and/or pushing data to online data repositories (Horsburgh et al., 2019).

While several do-it-yourself (DIY) EC sensor designs are available (Neelamegam & Vasumathi, 2010; Chapin et al., 2014; Dean & Werner, 2016; Divić et al., 2020; Shi et al., 2021), these are usually based on two-electrode sensors. However, two-pole probes are subject to polarization and can be sensitive to fouling or electrode corrosion, making them inappropriate at the higher EC values typically encountered in marine or estuarine settings. Furthermore, recent evaluations of low-cost two-pole probes raise questions about their accuracy and/or linearity, particularly when EC is high (Chan et al., 2020; Mendez-Barroso et al., 2020). An alternative EC sensor design involves the use of four electrodes, with two electrodes providing current and the other two sensing the voltage drop within the fluid media (Shreiner & Pratt, 2004; Kuphaldt, 2019). Four-pole sensors are typically more expensive than two-pole sensors, and, perhaps for this reason, there is not as much information on their use in DIY settings. Online discussion sites such as the Cave Pearl Project, PublicLab, Hackaday, OpenCTD, and EnviroDIY typically only provide build instructions and code for 2-pole systems (although EnviroDIY provides code for interfacing its Mayfly Arduino-based datalogger with commercial 4-pole sensors that process data internally and then communicate the results with the logger). While there are a few lab-based validation studies of custom-built EC sensors (Ramos et al., 2008; Tejaswini et al., 2019; Shi et al., 2021), we are not aware of any studies that have attempted to validate measurements made using a DIY 4-pole EC sensor in realistic estuarine field settings.

The primary objective of this paper is to evaluate a simple microcontroller-based 4-pole EC sensor that can make EC measurements in estuarine and marine systems over day- to week-long deployments. Our EC sensing system requires only a microcontroller, a few resistors, wire, and four electrodes. Temperature can be measured using an optional negative temperature coefficient (NTC) thermistor. Our system allows a low-cost microcontroller to serve as a datalogger for either DIY or commercial 4-pole probes, so another objective of our study is the characterization of error associated with the microcontroller-based EC measurement algorithm.

We also developed code and build instructions for combining our DIY EC sensor with a low-cost MS5803-05 pressure/temperature sensor. MS5803 sensors have shown promise in a number of recent studies that evaluated their real-world performance (Beddows et al., 2018; Elsmore et al., 2020; Temple et al., 2020; Shi et al., 2021), and they are recommended for oceanographic measurements by the OpenCTD project (https://github.com/OceanographyforEveryone/OpenCTD). The MS5803-05 can read absolute pressure up to 5 bars and is thus appropriate for depth measurements up to approximately 40 m. This sensor can be mounted in the same housing as our EC sensor, thereby allowing construction of a self-contained conductivity-temperature-depth

(CTD) sensor. Our entire CTD sensor can be constructed in a few hours for under $100 USD.

We begin by describing our EC sensor's principal of operation, basic build procedures, and the methods we used for calibration and field validation. We then present calibration curves obtained from four separate prototypes as well as field data collected from an estuary by these sensors and a co-located commercial reference device. We discuss challenges presented by DIY sensors and provide a few practical pointers and potential optimizations that may be useful for anyone interested in reproducing our work.

Methods

Much of the work developing the device was done in preparation for an undergraduate laboratory course in environmental sensors at Seattle University. Design priorities included minimizing cost and simplifying assembly so that students could create a working device during several lab sessions. To simplify construction, we developed designs for a 3-D-printed cap and two optional printed circuit boards (PCBs) that simplify assembly.

Development was done using MicroPython on the MicroPython reference circuit board, a pyboard (v.1.1). The pyboard is an STM32F405-based microcontroller that provides built-in battery-based power management, an SD-card slot, several low-power sleep modes, and access to a real-time clock (RTC). Once a backup battery is added, the pyboard's RTC can maintain accurate time for many months even when power is lost from the main batteries. Programming can be accomplished simply by copying code to the device or the SD card directly from a PC's file management system. It is also possible to interact with MicroPython-based devices in real time using an integrated development environment (IDE) such as Thonny—this proved useful for collecting calibration data. While our code was developed with a specific microcontroller in mind, the measurement algorithm can easily be implemented on any microcontroller with at least three ADC pins. To illustrate its applicability across multiple platforms and to begin evaluating how hardware choices may influence measurement accuracy, we adapted the code to run on a Raspberry Pi Pico 2040 and present results obtained from both the pyboard and the Pico 2040.

Fundamentally, four-pole EC sensors operate by applying a voltage difference across two outer electrodes and then measuring voltage at two inner electrodes (Kuphaldt, 2019). In our system, a schematic for which is given in Fig. 1, current is measured by sensing the voltage drop across a resistor ($R2$) connected to one of the outer (charged) electrodes (e2 in Fig. 1). The ratio of current to voltage drop between electrodes e3 and e4 represents a measure of the conductance (units $S=\Omega^{-1}$) of the fluid media. In Fig. 1, the blue shaded area represents the fluid for which EC is to be measured, and the gray shaded areas represent the four electrodes. Fouling of the electrodes or polarization within the fluid can increase the effective resistance of the circuit, thus reducing the overall current flow. However, this is likely to produce a compensatory drop in voltage at the two inner electrodes, making the 4-pole design much more resistant to fouling or polarization than a 2-pole probe.

We adapted a DC-based approach to measuring electrical conductivity across a four-pole probe described by the National Institute of Standards and Technology (NIST) (Shreiner & Pratt, 2004). Our method creates short pulses of DC current by setting GPIO1 and GPIO2 high (i.e., to 3.3V) and low (i.e., to 0V), respectively (our + state), or low and high, respectively (our − state). Voltages V_{adc1}, V_{adc2}, and V_{adc3} are measured at ADC1, ADC2, and ADC3 (Fig. 1) immediately after a given GPIO pin state is specified. Because negligible amounts of current are required for the ADC measurements, any fouling of the inner electrodes is unlikely to appreciably affect the estimates of voltage drop between these electrodes. The cycle is repeated n times ($n = 12$ in testing), producing n ADC readings for each polarity. The frequency at which polarity changes depends on the speed of the microcontroller but was typically several thousand hertz. For each ADC at each polarity, data are filtered by discarding the lowest and highest quartiles and averaging the remaining values.

A current estimate, i, is obtained for each polarity from the filtered voltage drop V_{adc3} across resistor $R2$,

$$\begin{aligned} i^{+} &= \frac{V_{adc3}}{R2} \\ i^{-} &= \frac{3.3-V_{adc3}}{R2} \end{aligned} \quad (1)$$

where superscript "+" corresponds with the polarity state associated with GPIO1 set high and superscript "−" corresponds with the polarity state associated with GPIO1 set low. For each polarity state, the apparent resistance R across the EC cell is computed using

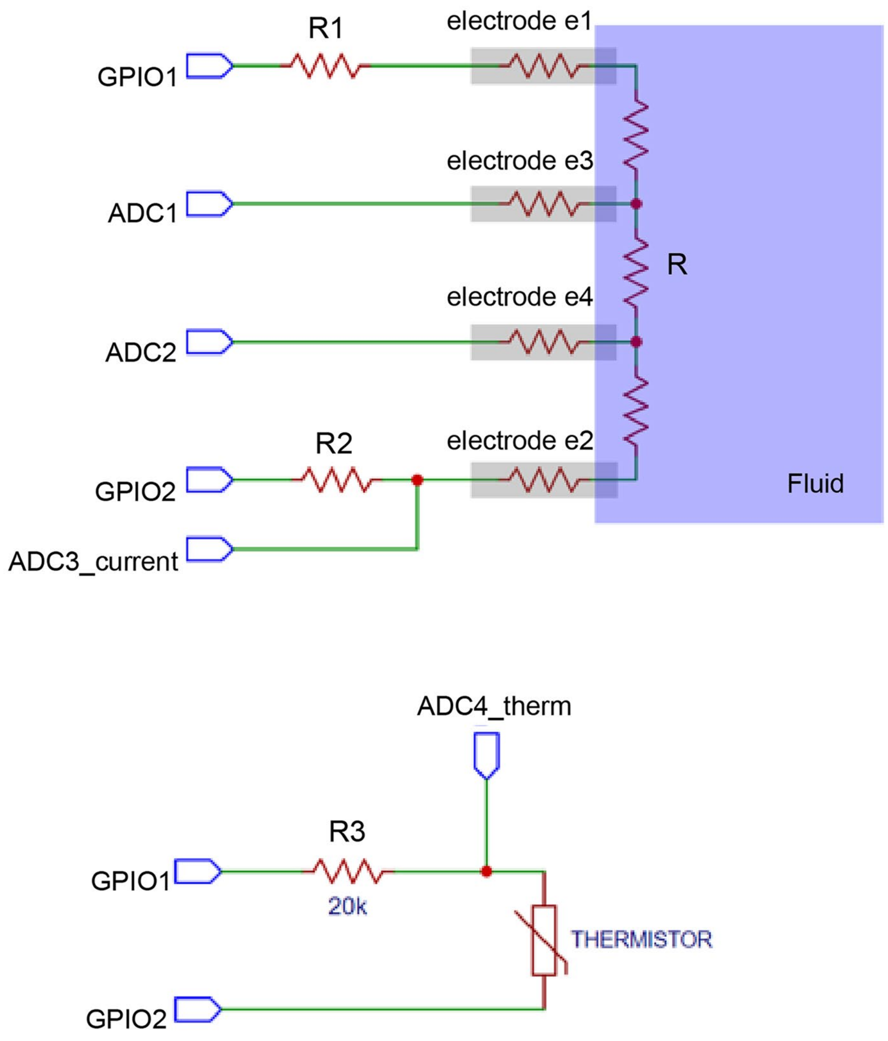

Fig. 1 Schematics for EC circuit (at top) and thermistor circuit (at bottom). The EC circuit is completed when electrodes e1 to e4 are immersed in the fluid media. When connected in parallel as illustrated, the EC/thermistor system requires a microcontroller with at least two available general purpose input output (GPIO) pins and four analog to digital (ADC) pins

$$R^+ = \frac{V_{adc1} - V_{adc2}}{i^+} \quad R^- = \frac{V_{adc2} - V_{adc1}}{i^-} \tag{2}$$

A calibration curve is then developed between the average of R^+ and R^-,

$$R = (R^+ + R^-)/2 \tag{3}$$

and the electrical conductivity as measured by a commercial device.

For an idealized EC cell, EC is inversely proportional to R and directly proportional to a cell constant K that depends on electrode geometry.

$$EC = \frac{K}{R} \tag{4}$$

We experimented with several materials for use as electrodes. Graphite in the form of 2-mm diameter pencil lead proved to be convenient, low cost, and relatively durable. This was used in three of our four prototypes (sensors SU1, SU2, and SU5). We also tested nickel-chromium (nichrome) wire in one of our sensors (sensor SU3). Electrical connections were made by wrapping wire around the electrode material and securing it using heat shrinkable wire crimp connectors and epoxy.

For prototypes based on the pyboard (sensors SU1, SU2, and SU3), temperature was measured using a Littlefuse PS103J2 NTC thermistor mounted near the electrodes. As illustrated in Fig. 1, the NTC thermistor sub-circuit was connected in parallel with the

EC sub-circuit, allowing us to use just one additional microcontroller pin, ADC4_therm, for estimating temperature within the EC cell. Thermistor resistance is sufficiently high that the parallel connection is unlikely to appreciably affect current flow through the EC circuit. For the prototype based on the Raspberry Pi Pico 2040, all three available ADCs were utilized in the EC sub-circuit, so temperature was measured using the internal temperature sensor on the MS5803-05 pressure sensor.

After laying out the electrodes and sensors for our first prototype (sensor SU1) in holes hand-drilled into a PVC pipe, we realized that construction could be simplified using standardized housings. We developed two 3-D printable housing designs, one that separates the EC electrodes/thermistor from the pressure sensor (used in SU2 and SU3) and one that reduces overall sensor size by including a port for the pressure sensor in the EC sensor housing (used in SU5). Figure 2 presents photographs of each prototype. Because each of our prototypes used a different combination of material and electrode geometry, the relationship between R and EC varies modestly from sensor to sensor. Housing designs and MicroPython code are available at https://github.com/jwlauer/CTD.

Calibration methods. We calibrated each device prior to deployment using EC measured by a YSI EXO-3 multiparameter sonde. Data were collected by placing the EXO-3 probe in approximately 500 mL of solution, slowly moving the probe to ensure well-mixed conditions, waiting several seconds until EC appeared stable, and then recording the reported EC and temperature. The EXO-3 probe was then removed and one or more readings were made using the DIY sensor. The EC solution was then diluted and the process repeated at the new EC value. Sensors SU1, SU2, and SU3 were built more than a year before sensor SU5 (a 4th sensor, sensor SU4, was damaged during or after a deployment, probably because of a bad solder connection). In the case of sensor SU1, the initial calibration was based on mixtures of table salt and tap water. All subsequent calibrations were done using KCl solutions mixed using deionized or distilled water. For the first three sensors, initial calibration data were collected soon after sensor construction over a somewhat variable EC range. For sensor SU1, initial calibration data fell within an EC range of approximately 0.06 to 90 mS/cm. For sensors SU2 and SU3, both of which were initially built and calibrated primarily in support of undergraduate student class projects, the initial calibration was limited to an EC range of between 0.1 and 11 mS/cm. To standardize

Fig. 2 Photograph of each prototype sensor. Note that the color of the potting epoxy used to waterproof the electrodes varies

the EC calibration, data were collected again on March 18, 2021, after sensor SU5 had been constructed and over a year after the initial calibration for sensors SU1 to SU3. Here, data were collected in triplicate at ECs between approximately 0.02 and 45 mS/cm.

As a test of overall sensor robustness, we developed calibration curves using all calibration data that was collected for each sensor. These overall calibrations utilized both 2020 and 2021 data and thus may not be appropriate for use in interpreting field data collected in 2021. For this reason, we also developed separate calibrations using only 2021 data. Some calibration data may have extended beyond the useful EC range of some of the sensors. For the 2021 calibrations, we considered the likely range of applicability for our sensors and excluded data from outside this range.

We identified the approximate sensor range by theoretically considering how the sensitivity of the sensor likely varies with EC. For the analysis, we assume that the resistance internal to the electrodes themselves is small and that the resistance in the fluid media between the charged electrodes el and e2 can be represented as K/EC. Under these assumptions, for the positive polarity case, the voltage measured by the current sensing resistor, V_{adc3}, is

$$V_{adc3} = 3.3\left(\frac{R2}{R1 + R2 + K/EC}\right) \tag{5}$$

because the estimate of R in Eq. (3) depends inversely on i and thus also on the inverse of V_{adc3}, lack of sensitivity of V_{adc3} to EC at the low end of the EC range, where i is low, is probably a significant source of sensor imprecision. Equation 5 can be used to evaluate how the relationship between a change EC and a commensurate change in V_{adc3}, that is, dV_{adc3}/dEC, varies with EC. This relationship is illustrated in Fig. 3, both in terms of millivolts per percent change in EC and in equivalent counts of the 12-bit ADC per percent change in EC. Sensitivity depends on EC, cell constant, and the value of resistors $R1$ and $R2$. Changing the cell constant or resistance shifts the point of maximum sensitivity towards higher or lower EC values but does not affect the overall range of the instrument. For an EC sensor with a cell constant $K = 1.0$ (close to our target cell constant) and $R1 = R2 = 250\,\Omega$ (as in our prototypes), a 1% change in EC corresponds with at least one ADC count for ECs between about 0.11 and 36 mS/cm. Our oversampling/filtering algorithm addresses the relatively low resolution at either end of the EC range, allowing for measurements beyond these thresholds. However, the figure illustrates why a sensor optimized for the higher ECs typically encountered in marine or estuarine settings may be relatively imprecise at the low end of the EC range, where the inverse relationship between EC and current magnifies error. For this reason, and because we observed some scatter in calibration data at the lowest ECs in our calibration dataset, we elected not to use calibration data below 0.18 mS/cm when developing the 2021 calibration curves that we used for evaluating field data. Furthermore, one of our sensors, sensor SU3, exhibited noticeably increased imprecision for EC higher than 8 mS/cm. This may have been caused by the sensor's use of nichrome wire (rather than the graphite used in by all other sensors) as electrode material. For this sensor, the 2021 calibration curve was developed using only the calibration data associated with ECs below 8 mS/cm.

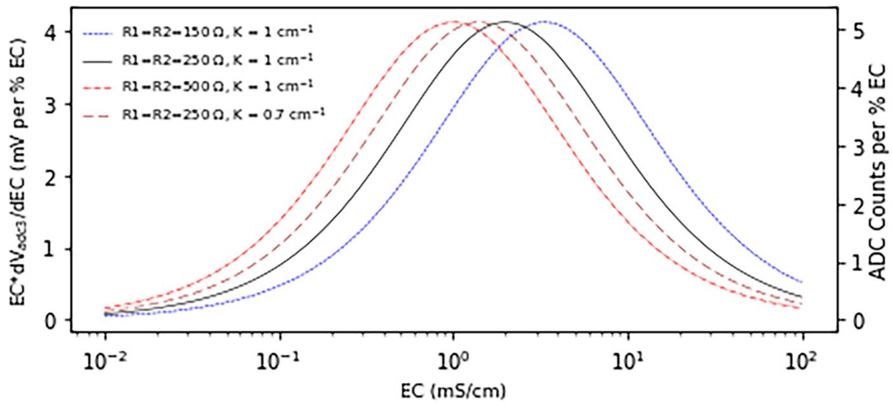

Fig. 3 Sensitivity of V_{adc3} to a 1% change in EC for several different sensor configurations

We fit calibration curves between the inverse of R and the observed EC measured by the YSI EXO-3 sonde using a three-parameter power function,

$$\frac{1}{R} = a(EC + c)^b \quad (6)$$

where a, b, and c are found through least-squares optimization. In cases where setting offset c to zero did not appreciably change the goodness of fit, we performed the analysis under the constraint that $c = 0$. For the overall calibrations performed using both 2020 and 2021 data, we also computed curves under the constraint that $b = 1$. For these curves, the inverse of parameter a represents an estimate of the sensor's cell constant K. For cases where the constraint $c = 0$ provided an adequate fit, we computed 95% confidence limits on the $\log(1/R)$ vs. $\log(EC)$ calibration curve according to equation 12 in Lavagnini and Magno (2007) and then took antilogs to transform the log confidence limits back to regular units. Where the calibration equation could only be fit well using a non-zero value for offset c, we first used least-squares optimization on un-transformed data to find c and then developed confidence limits on the relationship between $\log(1/R)$ and $\log(EC + c)$.

Study site/deployment The sensors were deployed in the Duwamish River near Seattle, Washington, USA (Fig. 4). The river downstream from the study site was straightened and dredged in the early 1900s to accommodate port development. Depths in the lower river are on the order of 4–5 m below mean lower low water (MLLW), producing strongly stratified conditions typical of salt-wedge type estuaries (McKeon et al., 2021). The tidal range of 3–4 m results in regular reversal in flow direction well upstream from the dredged portion of the river even during moderate to high river discharge conditions. The associated salt wedge can extend several kilometers upstream from the artificially deepened channel, although its maximum upstream extent depends both on tidal amplitude and river discharge.

Despite intense industrial use, the river supports significant populations of salmon. Management has

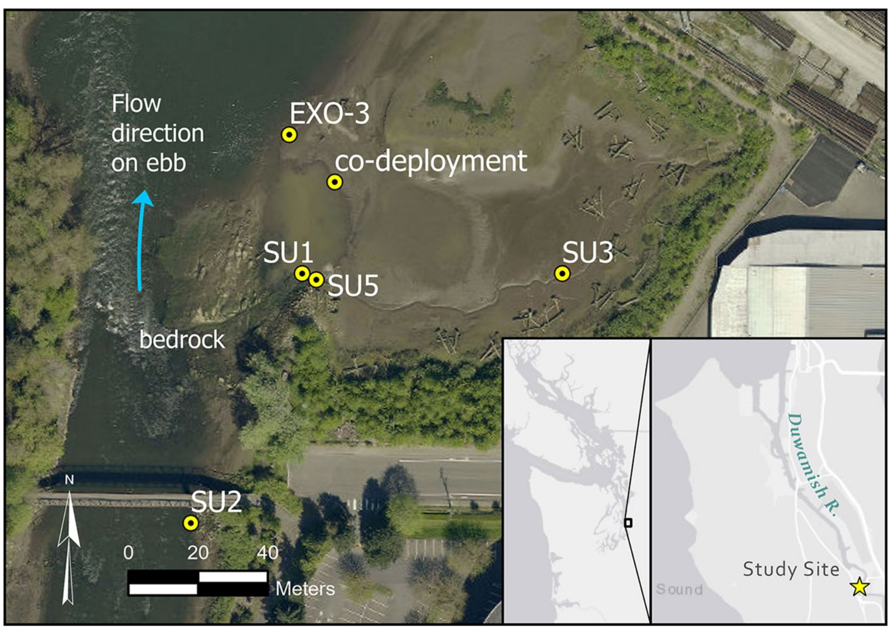

Fig. 4 Study site on the Duwamish River, Washington, USA. Points labeled SU1–SU3 and SU5 indicate the position of the DIY sensors and point EXO-3 indicates the position of the commercial sensor during the period when they were distributed across the site. During that period, sensor SU1 was located near SU5 but at a lower elevation. The co-deployment point indicates the location of all sensors during the periods when they were co-located (i.e., both before and after being distributed across the site). Background imagery was collected in 2015 during low tide. Erodible landforms may have shifted slightly by the time of the deployment

especially focused on endangered species act (ESA)-listed Chinook Salmon (Water Resource Inventory Area, 2005; Water Resource Inventory Area, 2021), which use the estuary at various stages of their life cycles, especially during out-migration in late spring. Growth rates for juvenile salmon are particularly high in relatively low salinity off-channel wetlands near the upstream end of the artificially dredged channel (Cordell et al., 2011), so several tidal wetlands have been constructed in this area (Simenstad et al., 2005). One of the largest is located immediately downstream from a natural bedrock outcrop known as North Winds Weir (NWW). NWW plays an important role in traditional Salish stories about the Duwamish River (Reese et al., 2016), so the bedrock was probably exposed even before industrial development of the lower river. Under existing conditions, the weir prevents stage in the upstream river from dropping below approximately 0.6 m above MLLW. Its influence on salinity dynamics within the nearby constructed wetland has not been extensively documented.

The spatial heterogeneity in the vicinity of the bedrock at NWW and the dynamic behavior of the salt wedge makes the NWW site a good location to validate our DIY EC sensors. During ebb at minus tides, a hydraulic jump forms as water crosses the bedrock. This maintains a pool immediately downstream from the bedrock. During minus tides, this pool receives flow primarily from the tidal channel draining the constructed wetland, possibly producing the turbidity visible in Fig. 4. We expected that the channel draining the tidal flat would provide relatively dense, high-EC water into the pool during low tide, leading to differences in salinity in the pool relative to the main river or the tidal channel. We also expected the arrival of the salt wedge upstream from the weir would be delayed relative to its arrival in the pool.

To test our sensors, we co-located them on a sand bar at the edge of the pool downstream from the bedrock sill, near the point labeled "co-deployment" in Fig. 4. Figure 5 shows a ground-based photograph of the co-deployment. Sensors were placed so that

Fig. 5 Photograph of co-located sensors immediately after deployment

their elevations varied by no more than 10 cm. The maximum horizontal distance between one sensor and any other was approximately 2 m. The sensors were left at this location for approximately 24 h and were then moved to the locations illustrated in Fig. 4, where temperature, EC, and depth were expected to experience distinctive patterns. Sensor SU1 was placed in the bed of the pool immediately downstream from the bedrock sill. Sensor SU2 was placed in about 0.9 m of water in the channel upstream from the bedrock sill. Sensor SU3 was placed in the tidal channel draining the tide flat at an elevation at least 1 m above where the co-located sensors had been deployed. Sensor SU5 was placed at the edge of the pool near the co-deployment point but closer to the mouth of the channel draining the tide flat. It was located a few meters horizontally from sensor SU1, so the main difference between these two sensors is elevation. The YSI EXO-3 was placed in the main river channel near the co-deployment point. Its position closer to the main river channel exposed it to much higher velocities, at least at low tide, than were present in the pool. Data were collected for approximately 24 h after the sensors were distributed across the site. The sensors were then moved back to their original co-located position, and data was collected for 2 additional days. Temperature data for each DIY sensor were corrected to match the EXO-3 temperature record by adding an offset computed from temperature data collected during the first few minutes of the first co-deployment period.

Results

Complete calibration data for all calibration datasets are presented in Fig. 6, along with the calibration

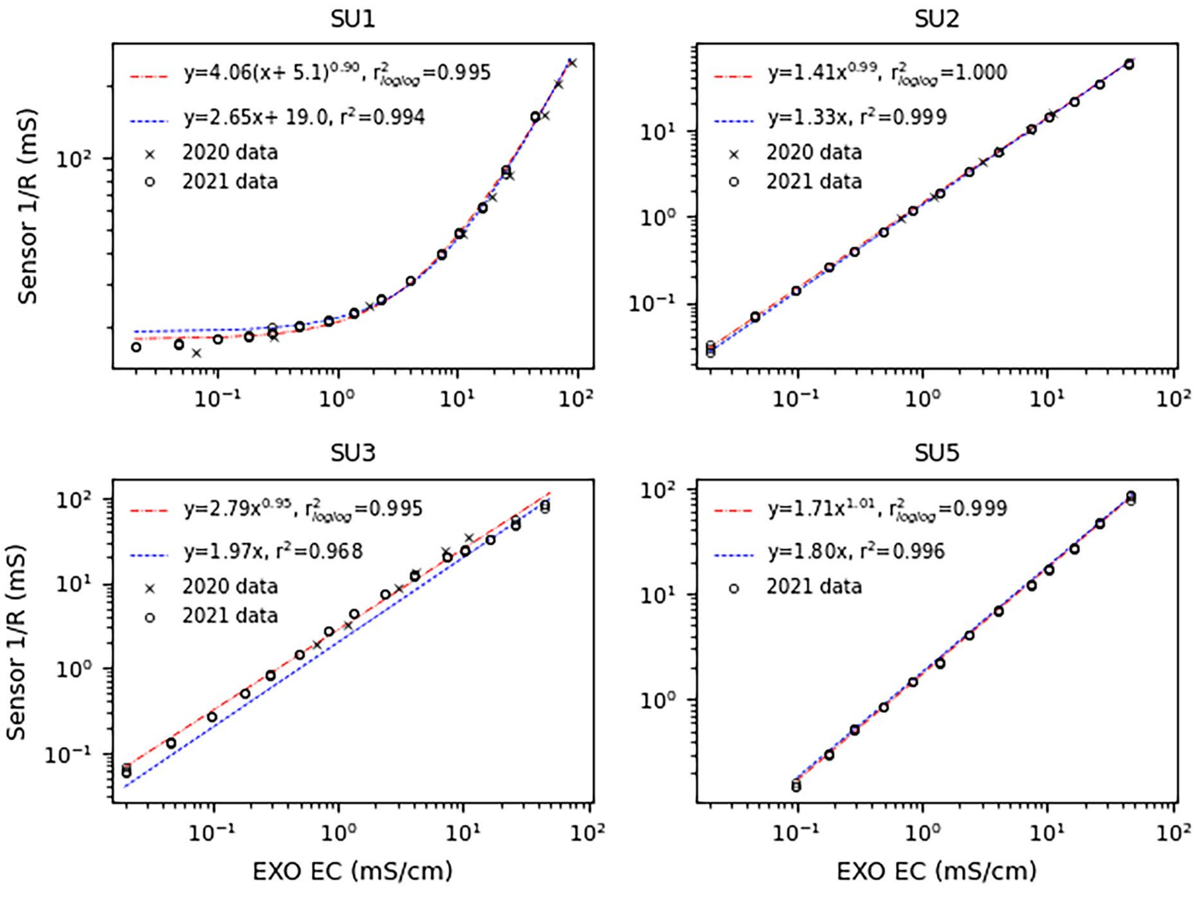

Fig. 6 All observed calibration data and best linear- and power-function fits for each sensor

curves fit to all the data. Note that data from sensor SU1 does not plot as a straight line in log-space because of the non-zero value of offset parameter *c*. The best-fit equations are provided in the figure, as are the values of the coefficients of determination computed from the linear regression (r^2) or the log-log regression (r^2_{loglog}) used to develop the best-fit power function. In all cases except the linear fit for sensor SU3, r^2 is better than 0.99. The worst fit was experienced for sensor SU3, where the data recorded for higher EC values appears to deviate from the trend present at lower EC values. The inverse of the slope of the regression line provides an estimate of the cell constant for each sensor. In all cases, cell constants were between 0.1 and 1. For the sensors where calibration data were collected in 2020 (i.e., SU1–SU3), the 2020 data are reasonably consistent with the 2021 data, particularly in the middle of the EC range.

Confidence limits on power-function calibration curves produced using the 2021 calibration datasets at EC above 0.18 mS/cm (sensors SU1, SU2, and SU4) or below 8 mS/cm (sensor SU3) are provided in Fig. 7. These charts are presented in non-log transformed coordinates in order to more completely visualize confidence limits at relatively high EC values. Coefficients of determination for the log-log regressions, r^2_{loglog}, are all higher than 0.995. Standard error, root mean square error (RMSE), and root mean square relative error (RMSRE) are also provided. For the best fitting sensor, SU2, the 95% confidence limits are approximately ±3% of the EC measurement.

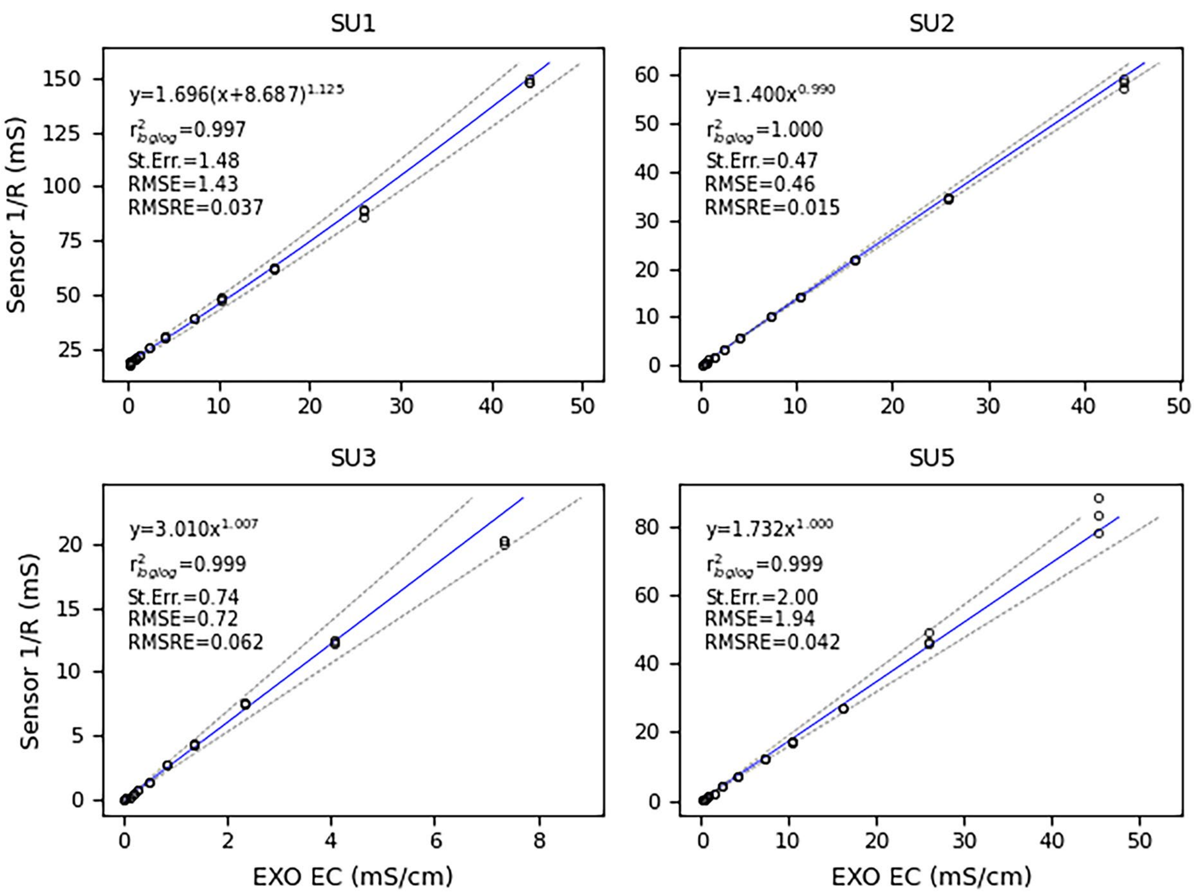

Fig. 7 Best-fit calibration equations and confidence limits constructed using 2021 calibration data. Note that a linear scale is used in order to highlight the size of the confidence limits at the higher end of the EC sensitivity range. Except in the case of sensor SU3, the calibration did not include points below 0.18 mS/cm. Sensor SU3, which appears to deviate from linearity at higher EC values (see Fig. 6), was calibrated using solutions with EC between 0.02 and 7.3 mS/cm

Results from the field deployments are given in Figs. 8, 9, and 10. In Fig. 8, time series of temperature, EC, and depth are presented for the periods when the sensors were co-located. The figure includes a roughly 24-h period starting on April 2, before sensors were distributed around the site, and a roughly 48-h period beginning on April 4, immediately after the sensors had been moved back to a common location. All sensors recorded a decrease in temperature and an increase in EC on the flood tide, then an increase in temperature and a decrease in EC during the ebb. In general, temperature and depth were consistent for all four sensors. In the case of EC, sensors SU1 and SU2 tracked the EC reading of the EXO-3 during flood more closely than did sensors SU3 and SU5, but the same general pattern of tidal fluctuation in EC was apparent in all sensors. For unknown reasons, the EC reading of sensor SU5, which had been set to record at 30-s intervals, exhibited variability of about 10 mS/cm at a relatively high frequency early on April 4, producing what appears to be a shaded region immediately before and after higher high water on that date. Sensors SU1, SU2, and SU3 had been set to record at 5-min intervals prior to the April 4–5 deployment, so their data does not appear as prominently in the figure until lower low water (LLW) on the 4th of April, when sensors SU2 and SU3 were collected and reprogrammed to record at 30-s intervals. Sensor SU1 recorded at 5-min intervals for the entire deployment period. Note that because sensors were moved during LLW on each tide, the relative positions of the sensors may have changed slightly over the course of the co-located deployment period.

Figure 9 presents EC from each DIY sensor plotted against data recorded by the EXO-3 device while the sensors were co-deployed. The EXO-3 signal has been interpolated linearly to provide estimates of the EXO-3 value at the times when the DIY sensors actually logged data. Data are denser for sensors SU2, SU3, and SU5 because they logged at 30-s intervals for at least part of the deployment.

Figure 10 presents data collected when the sensors were spread across the site at the locations shown in Fig. 4. In general, the data follow patterns similar to what was recorded when sensors were co-located, with increases in EC during flood and decreases during ebb. However, there are noticeable differences in temperature, EC, and depth patterns in each time series. The signal for sensor SU3 is the most distinctive, with much higher temperatures than at other sensors during periods when the tidal channel it was installed in was not inundated. A detailed discussion of these and other differences is provided below.

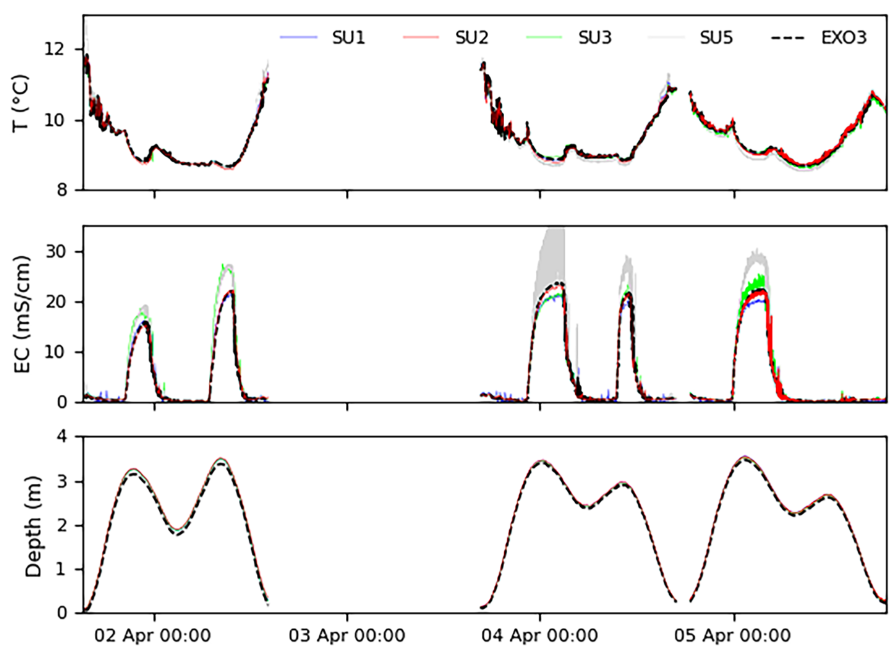

Fig. 8 Data recorded when sensors were co-located during April 1–5, 2021, deployment

Discussion

In this section, we first interpret the results of our deployment experiments. We then discuss the applicability of our sensors for other studies and provide some practical pointers for sensor construction.

Interpretation of deployment data

While there was modest variability in EC between sensors while co-deployed, the overall patterns are quite consistent with a highly stratified, salt-wedge type estuary. In Fig. 8, each tide was associated with one or more rapid transitions from fresh to near marine conditions and back. Tide records in Elliott Bay, near the mouth of the Duwamish River, indicate that the sensors were installed perhaps 10 to 20 cm below MLLW while co-deployed, an elevation well above the channel thalweg. The transition between river and marine salinity is thus apparently a daily occurrence across much of the channel boundary in this part of the estuary, at least for river discharges like those present during the deployment. Interestingly, despite only a modest decrease in lower high water (LHW) on April 5 relative to previous days, the salt wedge apparently did not enter the site during LHW on that day. River discharge at USGS gage 12113000, well upstream from tidal influence, varied by less than 5% over the course of the deployment, so the absence of marine water on April 5 highlights the complex, tidally driven variability in EC.

When distributed across the site, the sensors recorded subtle differences that depended on their position (Fig. 10). EXO-3 and SU5, both of which were deployed downstream from the bedrock outcrop within a few 10s of cm of MLLW, observed the

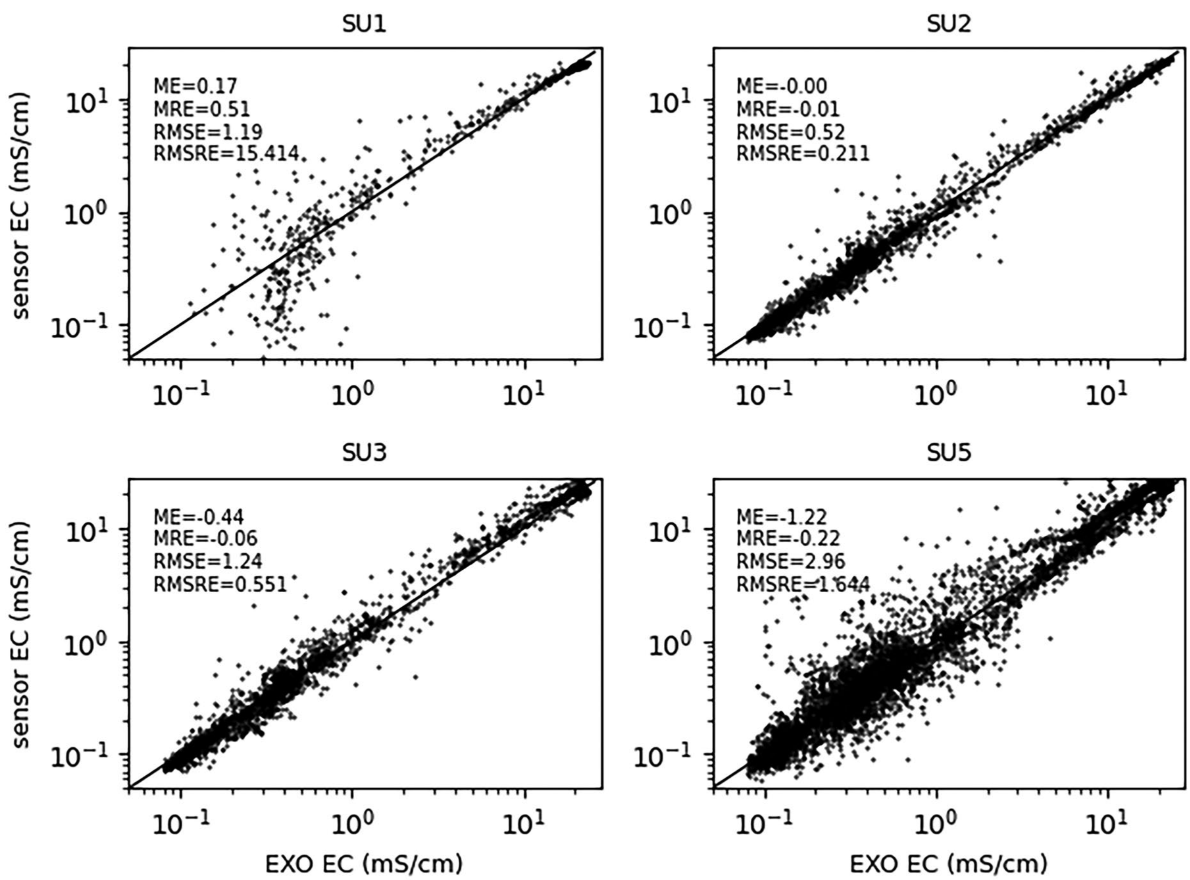

Fig. 9 Relationship between EC recorded by DIY sensors and EC recorded by YSI EXO-3 during period when sensors were co-located

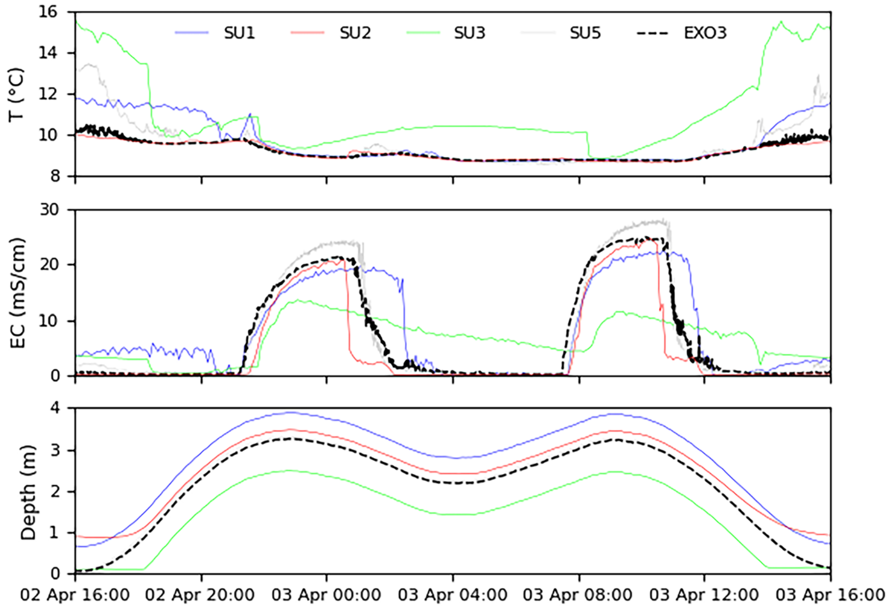

Fig. 10 Data recorded during April 2–3, 2021, deployment. Sensors were located at the positions shown in Fig. 7

relatively high-EC salt wedge for a similar amount of time on each high tide. However, at low tide, SU5 recorded much higher temperatures than those recorded by the EXO-3 device, probably because SU5 was located near the surface of the relatively quiescent pool that forms when water drops below the elevation of the bedrock outcrop. Warm drainage from the tidal flat enters this pool near the position of this sensor. Density-driven stratification probably persisted within this pool for much of the low tide. Sensor SU1, which was also deployed in this pool, but at an elevation nearly 1 m below SU5, observed moderate salinity during low tide, with EC on the order of several millisiemens per centimeter. Temperatures observed by SU1 within the pool early in the deployment were generally between those observed in the river by SU2 and EXO-3 and those observed near the pool's surface by SU5. However, as the flood progressed, temperature at SU5 actually fell below that at SU1, indicating that the stratification was driven primarily by salinity. During higher low water (HLW), both sensors within the pool (i.e., SU1 and SU5) observed similar temperatures and salinities as in the main river at SU2 and EXO-3. High-EC water persisted for SU1, at the bottom of the pool, much longer than at the other main-river sensors, but it too was eventually replaced by fresh river water.

Interesting differences were also observed between sensors SU1 and SU2. Both sensors were inundated to similar depths at low tide, but the position of SU2 in the main river channel upstream from the bedrock outcrop meant that low water conditions lasted much longer there than in the downstream pool because of the hydraulic control caused by the outcrop. There was no meaningful difference in peak EC upstream from the bedrock outcrop at the location of SU2 relative to the sensors that were installed in the main channel downstream from the bedrock (SU1, SU5, and EXO-3). However, the transition between low- and high-EC conditions occurred much more abruptly for SU2 than for EXO-3 or SU5. The rapidity of this transition can only have occurred if strongly stratified salt-wedge conditions were present upstream from the weir at high water. McKeon et al. (2021) documented a well-defined salt wedge in the Duwamish River downstream from our site. Our data imply that the salt wedge frequently extends well upstream from the dredged, artificially deepened portion of the estuary addressed by their study and that its upstream propagation may not be appreciably altered by the presence of the bedrock outcrop at the NWW site. However, the slower transition to freshwater conditions downstream from the weir could indicate that local turbulence may enhance mixing during the ebb.

The most unique pattern of EC and temperature was observed by sensor SU3, which was located about a meter in elevation above sensors SU5 and EXO-3, within a small channel draining the tidal flat.

Water flowing in this channel was sufficiently deep to keep the sensor submerged by a few centimeters during low tide, even when the rest of the flat had drained. During low tide, which occurred in the afternoon, temperature at SU3, and thus in water draining the flat, ranged from 14 to 16 °, much warmer than river water. Both days were warm and sunny, so the high temperatures in water flowing through the tidal channel were probably caused by solar heating of the flat. Warm tidal flat drainage entering the pool at the location of sensors SU1 and SU5 partly explains the relatively high temperatures observed by these sensors at low tide. Temperature in the tidal channel at SU3 dropped to 10 ° when the tide began to inundate the flat at about 18:00 on April 2.

Sensor SU3 also observed distinctive patterns of temperature and EC relative to all other sensors during the remainder of the deployment. During the flood (at least until HHW), EC at SU3 increased similarly to the other sensors. However, the brackish water was not washed out during the ebb as at all other sensors. Instead, EC gradually declined until it began increasing again during the flood preceding LHW. Temperature increased at SU3 during the ebb, leading to water that was several degrees warmer than at the other sensors until the next flood brought temperature back in line with sensors closer to the river. The increase in temperature during ebb could not have been caused by solar heating or by sensible heat exchange with the atmosphere because the warming occurred at night, when air temperature was well below the water temperature. This leads to the possibility that, at least within the small tidal channel draining the flat, there was some exchange between river water and a local source such as relatively warm, brackish groundwater. A groundwater source is also consistent with the moderate increase in EC observed at SU1 around LLW both on April 2 and April 3. During low tide, the small tidal channel at the site of SU3 is the only plausible source of brackish water for the pool in which SU1 and SU5 were located. The increase in EC deep in the pool, at the location of SU1, is consistent with this channel remaining a source of brackish water during the entire ebb (e.g., before 18:00 on April 2 and after 14:00 on April 3). However, the increases in EC at SU3 during flood occurred at around the same time EC increased elsewhere in the river, indicating that large-scale estuarine circulation, potentially moderated by local mixing at the bedrock outcrop, plays an important role in providing brackish water to the flat. Whatever the reason, the EC on the flat at the position of sensor SU3 remained much more consistent than at the other sensors during the periods when the flat was inundated. Outmigrating juvenile salmon in the Duwamish system may benefit from moderately brackish conditions (Cordell et al., 2011), so the muted EC range in this part of the restored wetland highlights the value of constructed off-channel habitats adjacent to parts of the river that experience large and rapid tidally driven fluctuations in salinity.

Application of DIY sensors for future work

In addition to the preliminary description of tidally driven salinity in a restored wetland, an important finding from our study is that excellent agreement is possible between a commercial sensor (the YSI EXO-3 multi-parameter sonde) and our DIY EC sensors. Furthermore, the precision of the 2021 calibrations for each of our sensors is remarkably good. In the case of sensor SU2, the error bands in Fig. 7 are consistently within ±3.2% of EC. This is close to the stated accuracy of lower-end commercial EC loggers such as those produced by Onset (3 to 5% accuracy for Hobo U24-002-C) or Solinst (±1 to ±2% accuracy for Levellogger 5 LTC), according to specifications published in the manufacturer's datasheets. Furthermore, it is notable that the temperature and depth fields for all sensors closely track the temperature and depth from the EXO-3 during all co-deployments, highlighting the robustness of the MS5803-05 pressure sensors (used for depth computations and for temperature measurements on sensor SU5), and of the Littlefuse PS103J2 NTC thermistor (used for temperature measurements on sensors SU1, SU2, and SU3).

Our results show that with proper calibration, DIY CTD sensors can collect meaningful data over timescales of at least several tides. Their construction can represent a far lower investment of resources than acquisition of a large number of commercial EC loggers. The rapid changes in polarity during measurement and the four-pole design mean they are more resistant to polarization and/or fouling than two-electrode probes, making them better suited to field deployment. Their low cost potentially allows for distribution of many sensors across a site, providing the opportunity to characterize spatial variability across highly heterogeneous systems such as channelized tidal wetlands. They are particularly well-suited for use cases in which sensor recovery is somewhat uncertain, for example in unmoored floats or at heavily used sites where risk of tampering or theft makes deployment of more expensive sensors imprudent. A further advantage of our DIY sensor is the ability to support simple customizations that can provide maximum sensitivity in the EC range of greatest interest. The DIY sensors can also easily be interfaced with other low-cost sensors, potentially allowing the addition of GPS-based position, light, sound, and other parameters to the data log.

Long-term drift is an important issue that our work partly addresses. For sensors SU1, SU2, and SU3, our initial calibrations, performed in spring 2020, produced results that are generally quite similar to the spring 2021 calibrations (Fig. 6), indicating that repeated wetting and drying may not dramatically affect sensor response. However, the 2021 calibration curves are not identical to the 2020 curves. For all sensors where 2020 data were available, we quantified the change by computing the mean relative error between observed and calculated EC for all calibration data gathered in 2020 using the inverted form of the 2021 power-fit curves shown in Fig. 7. Mean relative errors computed in this way are 227%, −1.4%, and 0.4% for sensors SU1, SU2, and SU3, respectively. Differences between the 2020 and 2021 calibrations are particularly apparent for our first prototype, sensor SU1, wherein the two lowest-EC calibration points dominate the relative error. This is probably a result of the inclusion of the offset in the power function fit for this sensor and/or random error in the 2020 calibration dataset. If the two lowest 2020 EC observations are discarded, so that drift is only evaluated in the range between 1.8 and 91 mS/cm, the mean relative error between the 2020 data and 2021 calibration curve for SU1 decreases dramatically, to 7.7%. While apparent drift is not large for the other sensors, we note that the sensor built with nichrome wire electrodes (SU3) reported maximum EC values that were well above those observed by SU1, SU2, or the EXO-3 early in the co-location period but that were much closer to the values observed by the other sensors later in the deployment (Fig. 8). Sensors were moved slightly each day, so the differences could have been caused by subtle changes in sensor position. However, we cannot rule out the possibility that the calibration for this sensor changed moderately over the 4-day deployment period. If drift occurred, it could have been caused by corrosion of the electrodes, movement of the wire used for electrodes, fouling, or some other reason. Our second co-deployment shows that the sensors built using graphite-based electrodes experienced minimal drift (Fig. 8), so we do not recommend using wire electrodes in new designs unless additional testing is done to ensure long-term stability and unless care is taken to physically stabilize the wires.

The possibility of drift in DIY sensors inevitably raises questions about data quality, even if the lab-based calibration is good. For this reason, validating the calibration before and after each deployment is particularly important with DIY equipment. One approach for addressing drift involves bringing calibration fluid into the field and allowing the sensor to log several points from the calibration fluid at the beginning and end of a deployment. However, in many field settings, this will only be practical if the sensors are set to record at relatively short (<1 min) intervals. Alternatively, sensors can be co-located before and after a deployment with a higher-precision commercial device, as done in this study. Many potential users of low-cost sensors may not have access to the laboratory equipment or materials needed for precisely mixing calibration standards. Consequently, it is worth discussing simple calibration procedures here. A 0.1 molar KCl standard with specific conductance of approximately 1.3×10^4 μS/cm requires only 7.43 g KCl/L distilled water. Specific conductance for other KCl solutions can be computed using McKee (2009) or Miller et al. (1988).

Ideally, calibration procedures and data should be stored as metadata along with any data record produced by a deployment of a DIY EC sensor. At a minimum, the date and time of any pre- and post-deployment calibrations, along with the concentrations and instrument readings, should be presented. This can be facilitated by the CalibrationActions portion of the ODM2 data standard (Horsburgh et al., 2016), or by uploading with measurement notes that document calibration data to an ODM2 data sharing portal (Horsburgh et al., 2019).

Practical pointers regarding sensor construction

Several of the sensors described in this study were built by undergraduate students who invested no more than 10 h into the construction of a given sensor. However, this is only after very extensive trial and error. Several practical issues are worth discussing.

Housing construction. While a standard 3-inch or 4-inch PVC pipe can be used for housing, it is far easier to confirm that the sensor is working properly if the built-in LED on the microcontroller is visible. For this reason, using clear PVC, as shown for SU2, SU3, and SU5 in Fig. 2, is a huge advantage. Clear PVC also simplifies testing for waterproofing.

SD storage. A notable advantage of MicroPython on the pyboard over other development environments such as Arduino is the ability to program the device simply by copying code to an SD card. Unless the data logging interval needs to be updated, no other programming is required, and data will automatically be logged to the SD card. Code can also be uploaded directly to flash memory, but in this case, downloading data will require a cabled connection to a computer.

Waterproofing. We found that the most reliable way to waterproof our housing was to use flexible rubber pipe cap and pipe clamps. Inside the housing, we recommend liberally applying 2–3 cm of potting compound around all points where wires penetrate the housing.

Time. Keeping accurate time can be a challenge with long-term deployments for any low-cost sensing project. Timing is one of the reasons we elected to use the pyboard. The internal RTC on the STM32F405 can be calibrated in MicroPython to within a few minutes per year. In addition, if an external coin cell battery is connected to the "vback" pin on the pyboard, the device will keep time for over a year even when the main power source is removed. We did not test RTC accuracy on the Pico 2040, but the similarity in timeseries collected by SU5 and the other sensors implies it is adequate for a several-day deployment.

Electrodes. The greatest challenge with the graphite electrodes we used in sensors SU1, SU2, and SU5 is making an electrical connection. Neither soldering nor crimping is feasible for graphite electrodes, so we simply wrapped wire around the graphite and then used a hot-melt impregnated shrink tube to mechanically reinforce the connection. Connections were then fully encased in potting material as part of the waterproofing process. This proved to be quite stable mechanically but takes some practice to perfect.

While our data indicate that the electrode geometry we settled on in the 3-D-printed electrode housings produces a cell constant that is useful for estuarine measurements, we did not exhaustively consider all possibilities. The spacing between electrodes was intended to produce a sensor with a cell constant of approximately 1 cm^{-1}. However, our calibration curves show that the cell constants were closer to 0.5 cm^{-1}. Increasing the cell constant by further optimizing the position and length of the electrodes could address this, as could optimizing the size of the resistors in the circuit. Figure 3 implies that even a minor shift in cell constant could provide additional sensitivity in the 10 to 40 mS/cm range common in many estuaries. Other combinations of electrode geometry and current-sensing resistor may be more appropriate in fully marine or fully fresh-water systems. It would be quite simple to add a mechanical switch to change sensitivity, e.g., by swapping between 1000 Ohm, 250 Ohm, and 100 Ohm values for $R1$ and $R2$.

While we tried a number of different low-cost electrode materials, other materials may perform better. While graphite proved relatively stable over time, it is brittle, and we did chip several electrodes during construction. A broken graphite electrode requires recalibration, so more durable electrodes could be helpful. However, the device we built with nichrome wire (SU3) experienced more drift in its calibration than did the sensors with graphite electrodes.

Microcontroller. Our development of sensor SU5 on a Raspberry Pi Pico 2040 shows that our code can easily be adapted for use on a range of microcontrollers. A version of the pyboard (the pyboard D) with wireless and Bluetooth hardware should be able to run our code with virtually no modifications. Using the pyboard D, it would be relatively straightforward to create a wifi-based interface for serving the data collected by the sensor, thereby greatly simplifying collection of calibration data. Other microcontrollers such as an ESP32 should also be able to run our code and can provide a wireless user interface. We did not use the ESP32 because of questions about the linearity of the ESP32's ADC, but with appropriate calibration, it may be an appropriate low-cost choice. Finally, our algorithm is sufficiently simple that it should be straightforward to reproduce it in other development environments such as Arduino.

Our testing of the Raspberry Pi Pico 2040 suggests that the sensitivity of the ADC is an important issue. As illustrated in Fig. 3, at both high and low EC, ADC-based measurements of current become relatively imprecise, so a reduction in ADC precision likely reduces the useful measurement range of the EC sensor. The Raspberry Pi Pico 2040 ran into precision errors at higher EC than the pyboard-based sensors, probably because there is an known offset voltage of a few millivolts in the Pico 2040's ADC. This may explain the higher variability in sensor SU5 than in sensors SU1, SU2, or SU3. However, the range is still sufficiently large that it could be used in many estuarine settings.

The MicroPython code we developed for this project executes sufficiently quickly that there is the opportunity for additional oversampling in order to improve precision. This is particularly the case with the Pico 2040, which was able to switch polarity at a frequency of over 6kHz. Given this sampling rate, it should be possible to increase oversampling by more than an order of magnitude—to 500 or 1000 internal samples. The extent to which this is likely to stabilize measurements has not been explored.

PCB. After constructing a number of early prototypes, we found that a simple PCB greatly reduces the possibility of incorrectly wiring up a sensor. We also developed a separate small PCB that simplifies installation of the MS5803 pressure sensor in our 3-D-printed housing. The gerber files for these PCBs are available at https://github.com/jwlauer/CTD/tree/master/hardware.

Conclusions

In this study, we deployed four DIY conductivity-temperature-depth sensors in the estuary of the Duwamish River. Calibration data collected using a commercial sensor show the DIY sensors can achieve 95% confidence limits as good as ±3% within the range of ECs likely to be experienced in an estuary. All sensors collected similar time series when co-deployed, validating their appropriateness for field use. Co-location data collected after the deployment as well as sensor calibration datasets collected more than a year apart for three of the sensors indicate that long-term drift is relatively modest.

When distributed across a constructed wetland located near a natural channel-spanning bedrock outcrop, the sensors collected widely varying temperature, EC, and depth time series that illustrate the complexity of stratified circulation near the upper end of a salt-wedge dominated estuary. Data show that the bedrock outcrop does not halt the upstream progression of the salt wedge, at least for tide and river discharge conditions like those observed during the deployment. However, the local topography near the bedrock outcrop and within the constructed tidal flat produced quite heterogeneous EC/temperature patterns at different tidal phases. The muted range of EC observed on the flat relative to the main river highlights the potential ecological value provided by constructed off-channel wetlands in this system. The results also imply that local drainage from the flat provides relatively saline water to parts of the estuary even when the river discharge is entirely fresh, thereby potentially providing distinct microhabitats for aquatic organisms.

Acknowledgements This research was supported by USDA Forest Service, Pacific Research Station through Cooperative Agreement JV-11261975 and by an internal Seattle University undergraduate research gra We would like to thank students Jazmine Patten, Ruby Ranoa, and Michaela Plumage for building one of the CTD sensors. We are also grateful to Andrea Ogston, Hannah Glover, Evan Lahr, and Elizabeth Davis for comments and suggestions regarding data analysis. We also appreciate the comments of two anonymous reviewers, both of whom made suggestions that improved the paper.

Funding This research was supported by US Forest Service Cooperative Agreement JV-11261975. Funding was also provided by an internal Seattle University undergraduate research grant.

Availability of data, material, and computer code Computer code and the datasets used in this paper are available at https://github.com/jwlauer/CTD. This site also provides additional information regarding build instructions and recommended material suppliers.

Declarations

Conflict of interest The authors declare no competing interests.

References

Beddows, P. A., & Mallon, E. K. (2018). Cave Pearl data logger: A flexible Arduino-based logging platform for long-term monitoring in harsh environments. *Sensors*, *18*(2), 530. https://doi.org/10.3390/s18020530

Blackstock, J. M., Covington, M. D., Perne, M., & Myre, J. M. (2019). Monitoring atmospheric, soil, and dissolved CO_2 using a low-cost, Arduino monitoring platform (CO_2-lamp): Theory, fabrication, and operation. *Frontiers in Earth Science, 7*, 313.

Chan, K., Schillereff, D. N., Baas, A. C. W., Chadwick, M. A., Main, B., Mulligan, M., O'Shea, F. T., Pearce, R., Smith, T. E. L., van Soesbergen, A., Tebbs, E., & Thompson, J. (2020). Low-cost electronic sensors for environmental research: Pitfalls and opportunities. *Progress in Physical Geography: Earth and Environment, 45*(3), 305–338. https://doi.org/10.1177/0309133320956567

Chapin, T. P., Todd, A. S., & Zeigler, M. P. (2014). Robust, low-cost data loggers for stream temperature, flow intermittency, and relative conductivity monitoring. *Water Resources Research, 50*, 6542–6548.

Cordell, J. R., Toft, J. D., Gray, A., Ruggerone, G. T., & Cooksey, M. (2011). Functions of restored wetlands for juvenile salmon in an industrialized estuary. *Ecological Engineering, 37*, 343–353.

Dean, R. N., & Werner, F. T. (2016). A PCB environmental sensor for use in monitoring drought conditions in estuaries. *Journal of Microelectronics and Electronic Packaging, 13*, 182–187.

DeBell, T., Goertzen, L., Larson, L., Selbie, W., Selker, J., & Udell, C. (2019). Opens hub: Real-time data logging, connecting field sensors to google sheets. *Frontiers in Earth Science, 7*, 137.

Divić, V., Galešić, M., Di Dato, M., Tavra, M., & Andričević, R. (2020). Application of open source electronics for measurements of surface water properties in an estuary: A case study of river jadro, croatia. *Water*, 12(1), 209. https://doi.org/10.3390/w12010209

Elsmore, K., Gaylord, B., Byrnes, J. E. K., Miller, L. P., Lyman, T. P., Byrnes, J. E. K., & Miller, L. P. (2020). Open wave height logger: An open source pressure sensor data logger for wave measurement. *Limnology and oceanography, methods, 18*, 335–345.

Horsburgh, J. S., Aufdenkampe, A. K., Mayorga, E., Lehnert, K. A., Hsu, L., Song, L., Jones, A. S., Damiano, S. G., Tarboton, D. G., Valentine, D., Zaslavsky, I., & Whitenack, T. (2016). Observations data model 2: A community information model for spatially discrete earth observations. *Environmental Modelling & Software, 79*, 55–74.

Horsburgh, J. S., Caraballo, J., Ramirez, M., Aufdenkampe, A. K., Arscott, D. B., & Damiano, S. G. (2019). Low-cost, open-source, and low-power: But what to do with the data? *Frontiers in Earth Science, 7*, 67.

Kuphaldt, T. (2019). *Lessons in Industrial Instrumentation*. http://www.ibiblio.org/kuphaldt/socratic/sinst/. visited 2021-03-10.

Lavagnini, I., & Magno, F. (2007). A statistical overview on univariate calibration, inverse regression, and detection limits: Application to gas chromatography/mass spectrometry technique. *Mass Spectrometry Reviews, 26*, 1–18.

Levine, R., Seroy, S., & Grünbaum, D. (2020). Sound and the seafloor: Determining bathymetry using student-built acoustic sensors. *Oceanography, 33,* 71–77. https://doi.org/10.5670/oceanog.2020.305

Mao, F., Khamis, K., Krause, S., Clark, J., & Hannah, D. M. (2019). Low-cost environmental sensor networks: Recent advances and future directions. *Frontiers in Earth Science, 7*, 221.

McKee, C. B. (2009). An accurate equation for the electrolytic conductivity of potassium chloride solutions. *Journal of solution chemistry, 38*, 1155–1172.

McKeon, M. A., Horner-Devine, A. R., & Giddings, S. N. (2021). Seasonal changes in structure and dynamics in an urbanized salt wedge estuary. *Estuaries and Coasts, 44*, 589–607.

Mendez-Barroso, L. A., Rivas-Marquez, J. A., Sosa-Tinoco, I., & Robles-Morua, A. (2020). Design and implementation of a low-cost multiparameter probe to evaluate the temporal variations of water quality conditions on an estuarine lagoon system. *Environmental Monitoring and Assessment, 192*.

Miller, R. L., Bradford, W. L., & Peters, N. E. (1988). Specific conductance: Theoretical considerations and application to analytical quality control. Water Supply Paper 2311. United States Geological Survey.

Neelamegam, P., & Vasumathi, R. (2010). Atmega32 microcontroller based conductivity measurement system for chloride estimation of soil samples. *Instruments and Experimental Techniques, 53,* 591–595.

Ramos, P. M., Pereira, J. M. D., Ramos, H. M. G., & Ribeiro, A. L. (2008). A four-terminal water-quality-monitoring conductivity sensor. *IEEE Transactions on Instrumentation and Measurement, 57*, 577–583.

Reese, T., Wagner, E., & Rasmussen, J. (2016). *Once and Future River: Reclaiming the Duwamish*. Seattle: University of Washington Press.

Seroy, S. K., Zulmuthi, H., & Grünbaum, D. (2020). Connecting chemistry concepts with environmental context using student-built pH sensors. *Journal of Geoscience Education, 68*, 334–344.

Shi, B., Catsamas, S., Kolotelo, P., Wang, M., Lintern, A., Jovanovic, D., Bach, P. M., Deletic, A., & McCarthy, D. T. (2021) A low-cost water depth and electrical conductivity sensor for detecting inputs into urban stormwater networks. *Sensors*, *21*.

Simenstad, C., Tanner, C., Crandell, C., White, J., & Cordell, J. (2005). Challenges of habitat restoration in a heavily urbanized estuary: Evaluating the investment. *Journal of Coastal Research*, SI 40, 6–23

Shreiner, R., & Pratt, K. (2004). Standard reference materials: Primary standards and standard reference materials for electrolytic conductivity. NIST Special Publication 260–142. National Institute of Standards and Technology.

Tejaswini, K. K., George, B., & Kumar, V. J. (2019). Conductivity measurement using non-contact potential electrodes and a guard ring. *IEEE Sensors Journal, 19*, 4688–4695.

Temple, N. A., Webb, B. M., Sparks, E. L., & Linhoss, A. C. (2020). Low-cost pressure gauges for measuring water waves. *Journal of Coastal Research, 36*, 661–667.

Water Resource Inventory Area 9. (2005). Salmon habitat plan - Making our watershed fit for a king. King County Water and Land Resource Division.

Water Resource Inventory Area 9. (2021). Salmon habitat plan 2021 update. King County Water and Land Resource Division.